A Case Study of Nearshore Drag Coefficient Behavior during Hurricane Ike (2008)

BRIAN C. ZACHRY* AND JOHN L. SCHROEDER

Wind Science and Engineering Research Center, Texas Tech University, Lubbock, Texas

ANDREW B. KENNEDY AND JOANNES J. WESTERINK

Department of Civil and Environmental Engineering and Earth Sciences, University of Notre Dame, Notre Dame, Indiana

CHRIS W. LETCHFORD

Department of Civil and Environmental Engineering, Rensselaer Polytechnic Institute, Troy, New York

MARK E. HOPE

Department of Civil and Environmental Engineering and Earth Sciences, University of Notre Dame, Notre Dame, Indiana

(Manuscript received 30 November 2012, in final form 26 March 2013)

ABSTRACT

Over the past decade, numerous field campaigns and laboratory experiments have examined air–sea momentum exchange in the deep ocean. These studies have changed the understanding of drag coefficient behavior in hurricane force winds, with a general consensus that a limiting value is reached. Near the shore, wave conditions are markedly different than in deep water because of wave shoaling and breaking processes, but only very limited data exist to assess drag coefficient behavior. Yet, knowledge of the wind stress in this region is critical for storm surge forecasting, evaluating the low-level wind field across the coastal transition zone, and informing the wind load standard along the hurricane-prone coastline. During Hurricane Ike (2008), a Texas Tech University StickNet platform obtained wind measurements in marine exposure with a fetch across the Houston ship channel. These data were used to estimate drag coefficient dependence on wind speed. Wave conditions in the ship channel and surge level at the StickNet location were simulated using the Simulating Waves Nearshore Model coupled to the Advanced Circulation Model. The simulated waves were indicative of a fetch-limited condition with maximum significant wave heights reaching 1.5 m and peak periods of 4 s. A maximum surge depth of 0.6 m inundated the StickNet. Similar to deep water studies, findings indicate that the drag coefficient reaches a limiting value at wind speeds near hurricane force. However, at wind speeds below hurricane force, the drag coefficient is higher than that of deep water datasets, particularly at the slowest wind speeds.

1. Introduction

Over 37 million people currently live in hurricane-prone coastal regions stretching from Texas to North Carolina and a continued increase in population is inevitable. As a result, there is an urgent need for nearshore observations of surface layer quantities to improve hurricane storm surge forecasting and to accurately define wind-loading provisions in the American Society of Civil Engineers (ASCE) standard for this critical region. Over the past decade, numerous field and laboratory experiments have examined air–sea momentum exchange in the deep ocean during hurricane conditions, but there is a significant gap in our understanding in shallow water and near the coast.

The transfer of momentum from the air to the sea is described in terms of a 10-m drag coefficient C_D defined as

$$C_D = \tau_o/(\rho_a \overline{U}_{10}^2) = u_*^2/\overline{U}_{10}^2, \quad (1)$$

where ρ_a is the density of air, τ_o is the surface wind stress, u_* is the shear velocity, and U_{10} is the mean wind speed

* Current affiliation: National Hurricane Center, Miami, Florida.

Corresponding author address: Brian C. Zachry, Storm Surge Unit, National Hurricane Center, Miami, FL 33165.
E-mail: brian.zachry@noaa.gov

DOI: 10.1175/JAMC-D-12-0321.1

© 2013 American Meteorological Society

measured at 10 m. Powell et al. (2003) and Donelan et al. (2004) found that C_D increases with increasing wind speed and reaches a limiting value of around 0.0025 near hurricane force. Black et al. (2007) found that C_D saturates to a value of 0.0018 at wind speeds of 22–23 m s^{-1}. The limiting nature of the drag coefficient has been attributed to the effects of spray droplets acting to limit turbulent mixing along with surface tension effects associated with a surface emulsion consisting of a deep layer of foam, and in short-fetch conditions, saturation is likely a result of airflow separation from the dominant waves (e.g., Powell et al. 2003; Kudryavtsev and Makin 2007).

Near the shore, wave interaction with the local bathymetry causes wave conditions to be markedly different from those in deep water due to wave shoaling and breaking transformation processes. At present, nearshore wind stress is not completely understood and only a few studies exist on this topic. Anctil and Donelan (1996) observed increased drag over shoaling waves compared to both deep water and breaking waves in Lake Ontario. For wind speeds of around 14 m s^{-1}, they estimated the shoaling wave drag to be 0.0028, which is higher than deep water values at similar wind speeds. Data reported in Powell (2008) also suggest increased drag in the nearshore region. Based on these studies and the wave condition differences stated above, it is believed that deep water wind stress parameterizations do not allow for reliable estimation of the nearshore wind setup and are a potential culprit for the inaccurate predictions of storm surge.

The work presented here aims to advance our understanding of momentum exchange at the coast and in complex wave conditions. Rare measurements of hurricane winds in marine exposure were obtained by a Texas Tech University rapidly deployable surface weather observing station, termed StickNet (Weiss and Schroeder 2008), during the passage of Hurricane Ike in 2008. The StickNet platform was inundated by surge during the peak of the storm with a predominant wind direction arriving from the 3-km-wide Houston ship channel. The surge at the station and wave conditions in the channel were estimated using a coupled wave and circulation approach via Simulating Waves Nearshore (SWAN) and the Advanced Circulation Model (ADCIRC), denoted SWAN+ADCIRC (Dietrich et al. 2011a,b). This work examines coastal drag coefficient behavior for wind speeds reaching hurricane force.

2. Field instrumentation and surge hindcast

A total of 24 StickNet weather stations were deployed during Hurricane Ike. One of the StickNet platforms (denoted StickNet 110A) was deployed in an open grassy area in Fort Travis Seashore Park on the Bolivar Peninsula (29.363 708°N, 94.759 234°W), near Galveston, Texas, to measure onshore winds in the eyewall (Fig. 1). The wind data collected from StickNet 110A provide the foundation for this work. Wind speed and direction were measured at a height of 2.25 m with a sampling frequency of 5 Hz using an R. M. Young Co. wind monitor. The station was deployed about 90 m from the water at mean tide at an elevation of approximately 3.7 m relative to the North American Vertical Datum of 1988 (NAVD88). Ike's center of circulation roughly passed directly over StickNet 110A, allowing for "classic" time histories of wind speed and direction indicative of the passage of the hurricane eye (Fig. 2). During landfall of Ike's southern eyewall, wind directions were from 190° to 230°. The wind fetch was from the Gulf of Mexico, then across Galveston and Pelican Islands, across the Houston ship channel, and finally onto the Bolivar Peninsula, where the wind measurements were sampled (Fig. 3). The derived surface layer quantities presented below are representative of the flow transitioning over these surfaces and ultimately the wave roughness in the ship channel.

FIG. 1. StickNet 110A deployed in Fort Travis Seashore Park, Bolivar Peninsula, Texas, during Hurricane Ike (2008). The photograph was taken by the Galveston County Office of Emergency Management during retrieval of StickNet 110A facing southwest toward the Houston ship channel.

Unlike the open ocean where both National Oceanic and Atmospheric Administration buoys and rapid-response gauges (e.g., Kennedy et al. 2010) provided wave observations during Ike's landfall, no such gauges existed in the ship channel. Hence, the authors simulated the wave and surge conditions using a SWAN+ADCIRC hindcast of Hurricane Ike. The simulation was conducted on the SL16 + TX grid, which is an unstructured, finite-element mesh that contains 9 228 245 nodes and 18 300 169 elements. The hindcast was run for a total of 39 days,

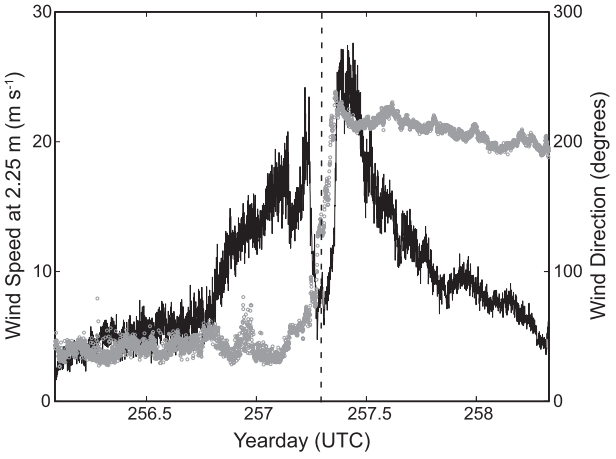

FIG. 2. Raw 1-min wind speed (black solid line) and wind direction (gray circles) time records (at 2.25 m) obtained from StickNet 110A during Hurricane Ike (2008). Landfall is denoted by the vertical dashed line.

which included Hurricanes Gustav and Ike and a spinup time of 18 days to allow the tidal signal to be replicated with constituents K1, O1, M2, S2, N2, K2, Q1, and P1. Surface stresses were calculated using an Ocean Weather, Inc., representation of the wind field (Powell et al. 1996, 1998, 2010; Powell and Houston 1996) and a drag coefficient formulation following Garratt (1977) with the radial dependence of Powell (2008). The drag coefficient formulation found herein was not applied in the hindcast due to the circular nature of this result and to the fact that a sensitivity study will be provided in a following paper. Initial water levels were raised by 0.280 m to adjust for seasonal expansion and the vertical datum adjustment, and the river flux in the Mississippi was set to 12 318 $m^3 s^{-1}$. Wave- and water-level properties were saved at hourly intervals for the analysis. A complete validation of the SWAN+ADCIRC hindcast is provided in Hope et al. (2013) in which they found the coefficient of determination to be 0.91 between the observed and modeled high-water marks.

The bathymetry of the channel is not representative of a typical shoreline, where waves propagate toward the shore from oceanic deep water. Near the edges the channel is shallow, but drops off quickly to approximately 14 m deep with a slope of 2.5:1. In the center of the channel (29.350 335°N, 94.771 247°W), the simulated waves were indicative of a fetch-limited condition with maximum significant wave heights reaching 1.5 m and peak periods of 4 s (Fig. 4). A maximum water level of 4.17-m NAVD88 was hindcast in the channel. At the StickNet, the simulated surge reached a height of 4.3 m NAVD88 or roughly 0.6 m above local ground, which is

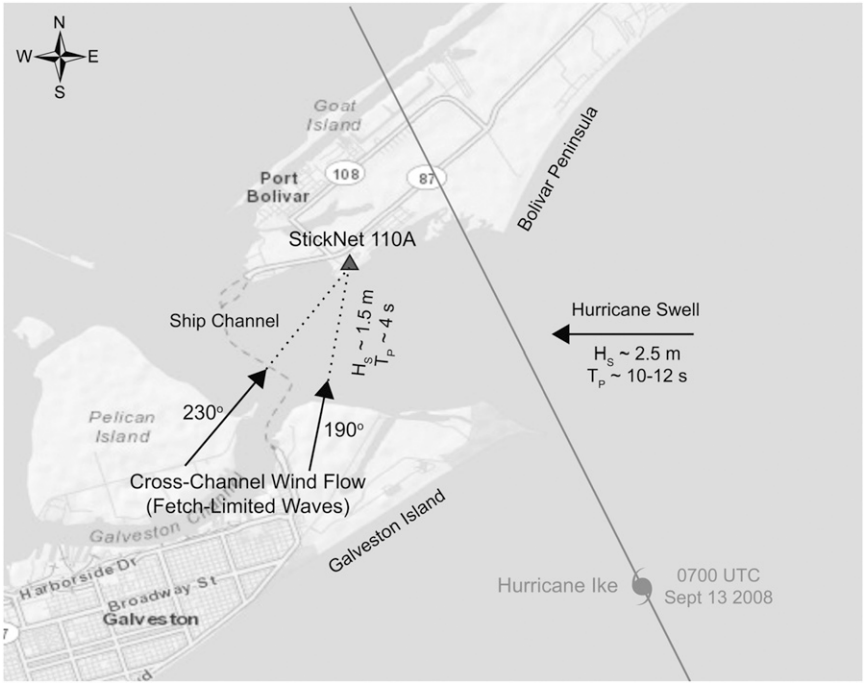

FIG. 3. The observed path of Hurricane Ike (2008), the wind fetch (wind directions of 190°–230°) used in the analysis, modeled wave heights in the ship channel using SWAN+ADCIRC, and observed waves offshore in the Gulf of Mexico.

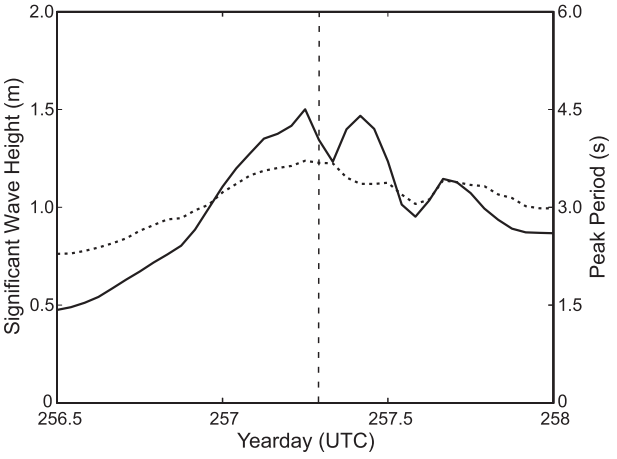

FIG. 4. SWAN+ADCIRC hindcast of significant wave height (solid line) and peak period (dashed line) in the center of the Houston ship channel during Hurricane Ike.

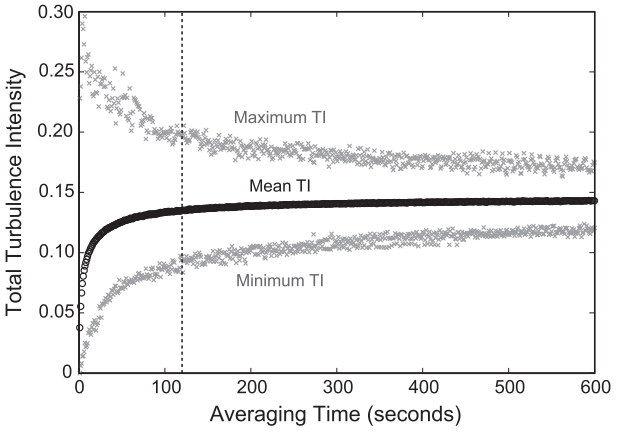

FIG. 5. Dependency of the total TI on averaging time. The 2-min averaging time used in this study is denoted by the vertical dashed line.

in agreement with a high-water mark of 0.6 m measured on the StickNet. In other words, roughly 1.65 m of StickNet 110A was above the water surface during the peak of the surge and hence the anemometer height was 1.65 m at this time.

3. Methodology

a. StickNet 110A wind measurements

StickNet 110A measured tropical cyclone winds with a fetch across numerous changes in land and marine exposures. Wind flow interaction with these varying surface roughness regimes leads to complex internal boundary layer (IBL) interaction and transition. Based on numerous relationships for IBL growth (e.g., Peterson 1969; Wood 1982; Arya 1988; Stull 1988; Kaimal and Finnigan 1994; Powell et al. 1996; Simiu and Scanlan 1986; Holmes 2001; Savelyev and Taylor 2005), and assuming the lowest 10% of the IBL depth is fully adjusted, StickNet 110A measured marine-type winds associated with the wave conditions (marine roughness) in the Houston ship channel. Many of the IBL growth equations provided in the literature are based on measurements for specific roughness transitions, and the authors are not generally aware of any literature that directly applies to the fetch scenario and wind speeds analyzed herein. Although unlikely, a minimal impact of the upstream roughness on the sampled IBL cannot be completely ruled out because of the complex IBL transition analyzed (e.g., Schmid and Oke 1990).

Since the StickNet stations only collect single-level u–v wind data, the turbulence intensity (TI) method was utilized to estimate the roughness length (Beljaars 1987). Turbulence intensity is a measure of the fluctuating component of the wind. In general terms, TI characterizes the intensity of gusts in the flow, and is defined as the ratio of the standard deviation of the fluctuating component of the wind to the mean wind speed. By substituting TI into the log law, z_o and C_D are computed as follows:

$$z_o = z_a \exp\left(-\frac{1}{\mathrm{TI}}\right) \quad \text{and} \quad C_D = k^2\left[\ln\left(\frac{z_a}{z_o}\right)\right]^{-2}, \qquad (2)$$

where $z_a = 2.25$ m is the anemometer height (on dry land) and $k = 0.4$ is the von Kármán constant. The TI method can be applied to wind data based on two main assumptions. First, this method assumes that a logarithmic wind profile exists. Overwater dropsonde data from Powell et al. (2003) and Powell (2008) show that a logarithmic wind profile exists in tropical cyclones. Second, the method assumes that the ratio of the standard deviation of the wind to the friction velocity is 2.5 (e.g., Counihan 1975; Beljaars 1987). Conceptually, this ratio simply states that boundary layer turbulence is purely driven mechanically with no contribution from buoyant processes. Although this ratio is well established in the published literature (e.g., Barthelmie et al. 1993, Letchford et al. 2001; Paulsen and Schroeder 2005), there is uncertainty around its value and future research projects aimed at establishing this are greatly needed. Regardless of the uncertainty in the 2.5 assumption, this ratio has provided comparable results to other methodologies (e.g., Barthelmie et al. 1993).

The TI varies based on averaging time (Schroeder et al. 1998). To determine where TI stabilizes, the wind speed record was windowed into various averaging times, and mean, maximum, and minimum values were computed (Fig. 5). An averaging time of 2 min was

utilized for this work (computed from the 5-Hz instantaneous measurements), as this window length captures variations in the smaller scales of motion, which are driven by surface roughness. Because of the sampling rate, wind gusts with frequencies greater than the Nyquist frequency of 2.5 Hz are inherently aliased. In addition, mechanical anemometers are not able to resolve all scales of motion, as the rotating components tend to filter the amplitudes of the highest-frequency gusts. Not resolving the highest-frequency gusts likely yields a marginal reduction in the standard deviation of the fluctuating component and, hence, a smaller z_o value. This is a concern for all high-frequency wind measurements and is not unique to this work. Regardless of this limitation, TI becomes fairly stable by 2 min with only a modest increase of 6.0% from 2 to 10 min. Nonstationarities lead to anomalous TI values, and hence only stationary wind speed segments (in both the mean and variance), as evaluated using the reverse arrangement test at a significance level of $\alpha = 0.01$ (Bendat and Piersol 1986), were used in the analysis.

b. SWAN+ADCIRC wave and surge hindcast

The SWAN+ADCIRC hindcast provides a means to characterize the upstream wave roughness and the surge at the StickNet. It should be noted that the hourly output from SWAN+ADCIRC does not completely capture the complex wave conditions in the ship channel. Conceptually, there were two wave fields interacting: 1) swell that propagated into the ship channel from the Gulf of Mexico and 2) local wind-driven waves (which are captured in the hourly significant wave height), both of which contribute to the underling wave roughness. In addition to this highly complex interaction among the wave fields, local changes in bathymetry, interaction with breakwaters, refraction and diffraction, and strong currents complicate the wave conditions.

Since the StickNet was inundated by surge (see Fig. 6), an additional scaling factor is necessary to determine the wind characteristics. The water rise acts to change the theoretical height of the anemometer relative to the ground–water surface. Any depth of water lowers the measurement height and subsequently (without adjustment) lowers the computed z_o, enhances the 10-m estimated wind speeds, and lowers the 10-m-derived C_D. Where indicated below, this scaling was applied using the time series of local water level hindcast by SWAN+ADCIRC.

4. Analysis and discussion

The drag coefficient was analyzed for three different time durations (Fig. 6). Over these time periods, the wind direction remained relatively stable with a fetch across the channel. Mean wind speed data obtained at 2.25 m (or a lower height based on the simulated water depth at the StickNet) were referenced to 10 m using the neutral-stability log law (Stull 1988), as follows:

$$C_{D(10)} = C_{D(2.25)}\left(\frac{\overline{U}_{2.25}}{\overline{U}_{10}}\right)^2. \quad (3)$$

Durations of 12 and 22 h were used to determine the dependence of the drag coefficient with wind speed. The longer record is provided to show differences at lower wind speeds, as the highest wind speeds occurred in the first few hours and the slowest near the end of the record. For the lower wind speed values in the 22-h duration, the wave heights and water levels had decreased in the ship channel, and more land was exposed on both the Bolivar Peninsula and Galveston Island based on the simulation. Surface layer quantities were also determined for the duration in which the StickNet was inundated by surge. Based on the hindcast, the StickNet was inundated for 1.03 h of the analysis length.

The standard way to assess C_D versus U_{10} is to partition the wind speed data and corresponding C_D values into bins with equal ranges. Six wind speed bins of $5\,\mathrm{m\,s^{-1}}$ were chosen ranging from 5 to $35\,\mathrm{m\,s^{-1}}$. It is assumed that if the number of data points in each bin is greater than 10, then a reasonable sample size has been achieved. Statistics for the different wind records binned into six wind speed groups are shown in Table 1. Wind

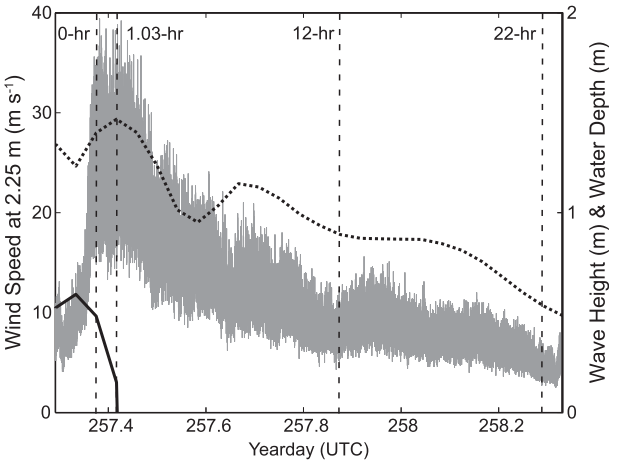

FIG. 6. Time series of wind speed (gray solid line), water level (black solid line), and significant wave height (dashed black line) used in the analysis. The 0-h vertical dashed line corresponds to the start of the record used in the analysis and the remaining vertical dashed lines correspond to analysis lengths of 1.03 h (during which the StickNet platform was inundated by surge based on the SWAN+ADCIRC hindcast), 12 h, and 22 h.

TABLE 1. Drag coefficient referenced to 10 m for different wind speed bins and record lengths. Values are also reported with and without the correction to the wind speeds via SWAN+ADCIRC hindcast water depths (indicated by the asterisk next to the wind speed bins affected by this correction).

Record	Statistic	U_{10} bins ($m\,s^{-1}$)							
		5–10	10–15	15–20	20–25	25–30	25–30*	30–35	30–35*
12 h	No. of 2-min segments	13	108	90	33	49	42	18	25
	Mean wind speed ($m\,s^{-1}$)	9.54	12.9	17.4	21.8	27.9	28.0	31.0	31.2
	Std dev wind speed ($m\,s^{-1}$)	0.326	1.50	1.50	1.33	1.41	1.47	0.812	0.971
	Mean wind direction (°)	211	213	219	214	217	216	220	220
	Std dev wind direction (°)	1.56	3.60	4.70	2.06	5.56	5.52	6.67	6.10
	Mean roughness length (mm)	0.760	1.68	1.77	2.14	2.37	1.87	2.11	2.23
	Std dev roughness length (mm)	0.710	1.66	1.25	1.63	1.86	1.29	1.37	1.85
	Mean drag coefficient $\times 10^3$	1.67	1.99	2.07	2.16	2.22	2.11	2.16	2.17
	Std dev drag coefficient $\times 10^3$	0.362	0.434	0.343	0.365	0.370	0.310	0.353	0.394
22 h	No. of 2-min segments	192	196	90	33	49	42	18	25
	Mean wind speed ($m\,s^{-1}$)	8.55	12.1	17.4	21.8	27.9	28.0	31.0	31.2
	Std dev wind speed ($m\,s^{-1}$)	1.07	1.50	1.50	1.33	1.41	1.47	0.812	0.971
	Mean wind direction (°)	200	210	219	214	217	216	220	220
	Std dev wind direction (°)	4.84	4.64	4.70	2.06	5.56	5.52	6.67	6.10
	Mean roughness length (mm)	1.32	1.68	1.77	2.14	2.37	1.87	2.11	2.23
	Std dev roughness length (mm)	1.26	1.65	1.25	1.63	1.86	1.29	1.37	1.85
	Mean drag coefficient $\times 10^3$	1.89	1.99	2.07	2.16	2.22	2.11	2.16	2.17
	Std dev drag coefficient $\times 10^3$	0.387	0.431	0.343	0.365	0.370	0.310	0.353	0.394
1.03 h	No. of 2-min segments	—	—	—	—	15	15	12	12
	Mean wind speed ($m\,s^{-1}$)	—	—	—	—	28.2	28.8	31.1	31.6
	Std dev wind speed ($m\,s^{-1}$)	—	—	—	—	1.08	1.07	0.777	1.019
	Mean wind direction (°)	—	—	—	—	223	222	225	225
	Std dev wind direction (°)	—	—	—	—	3.03	3.09	4.02	3.49
	Mean roughness length (mm)	—	—	—	—	2.72	2.03	2.19	1.97
	Std dev roughness length (mm)	—	—	—	—	1.82	1.51	1.31	1.06
	Mean drag coefficient $\times 10^3$	—	—	—	—	2.31	2.14	2.20	2.15
	Std dev drag coefficient $\times 10^3$	—	—	—	—	0.359	0.344	0.307	0.283

directions are very similar for the strongest wind speeds (within 20°), showing that a very similar fetch existed throughout the records. At slower speeds the winds have a greater southerly component. This result is due to the winds turning counterclockwise as the hurricane moved north of the region late in the record.

Binned drag coefficients are plotted against wind speed in Fig. 7. For the 12- and 22-h durations without correction for water levels at the StickNet, the drag coefficient increases with wind speed initially, reaches a limiting value of 0.0022 at a wind speed near $28\,m\,s^{-1}$, and decreases for wind speeds above $28\,m\,s^{-1}$. Compared to the 12-h record, the drag coefficient is higher at lower wind speeds for the 22-h record. For the 5–10 $m\,s^{-1}$ wind speed bin, this result could be due to small sample size or increased land exposure and hence roughness near the end of the record as the water receded from the Bolivar. When the correction for water level is taken into account, only the highest two wind speeds bins are affected. In the 30–35 $m\,s^{-1}$ wind speed bin, the drag coefficient increase minimally from the noncorrected analysis and in the 25–30 $m\,s^{-1}$ bin the values decrease more significantly. Regardless, a limiting value has been reached, but data at higher wind speeds would be necessary to confirm any trends beyond the threshold of hurricane force winds.

Drag coefficients in this complex environment are compared with previous studies in Fig. 7. The present work is consistent with the deep water studies in that C_D reaches a limiting value and either decreases or remains relatively constant for higher wind speeds. In regard to the wind speed that C_D saturates, the coastal drag coefficient reached a limiting value at slower wind speeds than Powell et al. (2003) and Donelan et al. (2004) and at faster wind speeds than Black et al. (2007). There are not sufficient data to compare the limiting values to the nearshore values presented in Powell (2008).

Examination of Fig. 7 also reveals that coastal C_D values are significantly higher for wind speeds of less than $25\,m\,s^{-1}$. Powell et al. (2003) and Powell (2008) indicate that deep and shallow water values decrease rapidly for wind speeds below hurricane force. Crudely extrapolating their results to slower winds, the drag coefficient would be markedly less than those obtained here during Hurricane Ike. Laboratory observations from Donelan et al. (2004) also indicate lower drags for

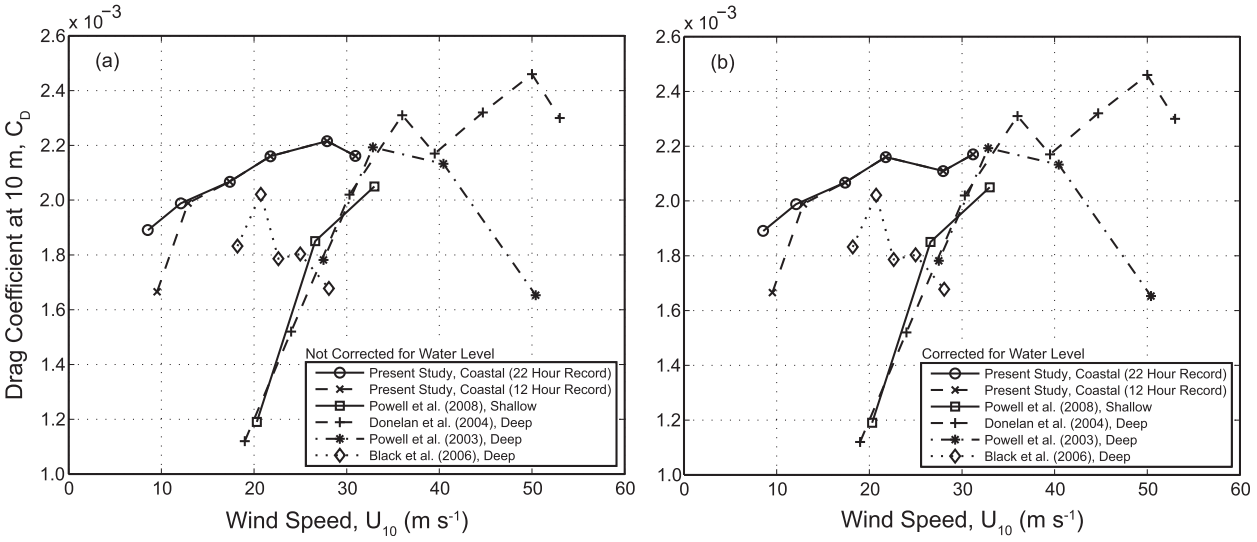

FIG. 7. Drag coefficient dependence on wind speed for this study: (a) wind speeds not corrected for water level and (b) wind speeds corrected for water level at the StickNet via SWAN+ADCIRC hindcast. Results are compared with shallow water values from Powell (2008), open-ocean measurements from Powell et al. (2003) and Black et al. (2007), and simulated extreme winds in the laboratory from Donelan et al. (2004). For Powell et al. (2003) the values are an average of the four mean boundary layer groups, and for Donelan et al. (2004) the values are based on the momentum budget method.

lighter winds and that the trend in C_D with increasing wind speed is much steeper than the present study. This result is likely a consequence of the fetch-limited and complex wave conditions in the ship channel generating a rough wave surface even under light-wind conditions.

5. Concluding remarks

Field observations of coastal wind measurements were obtained during the passage of Hurricane Ike. It was found that aerodynamic drag increased with wind speed up to 28 m s^{-1}, where a limiting value of 0.0022 is reached. When wind speeds are corrected based on the SWAN+ADCIRC hindcast water levels at the StickNet, the drag coefficient levels off at slower wind speeds of 22 m s^{-1}. These results are similar to deep water studies. Saturation of C_D is likely a result of sea spray and skimming flow as the waves are fetch limited and very steep. At slower wind speeds, the drag coefficient values are higher than those reported in any of the comparison deep water studies. This result could be a consequence of the complex wave conditions in the channel creating a ''rougher than normal'' surface under light to moderate winds. Similar relationships may also exist in regions that exhibit complex bathymetry, coastal formations that interfere with the local waves, or other types of fetch-limited conditions. Based on this analysis, storm surge models using a deep water wind speed–dependent drag coefficient may be slightly underestimating hurricane storm surge, and additional forcing parameterizations are needed in such complex roughness situations.

Based on recent air–sea interaction research, structures built on the hurricane-prone coast are currently being designed to withstand wind loads specified by Exposure D in ASCE 7-10 (i.e., flat, unobstructed areas and water surfaces with associated roughness lengths of 5 mm). The previous standard, ASCE 7-05, was set at Exposure C (i.e., open terrain with scattered obstructions having heights generally less than 9.1 m with associated roughness lengths of 20 mm). In other words, the hurricane-prone coast is now smoother from a roughness perspective and structures must be designed for higher wind loads (faster winds speeds). Data obtained during Hurricane Ike in complex nearshore conditions are in agreement with the shift to Exposure D in this region, as mean z_o values are on the order of 2 mm. These findings suggest that similar wave environments may also exhibit roughness values according to Exposure D. This work also adds to the literature base for ensuring reliable design standards in hurricane-prone regions for all wave conditions.

Acknowledgments. Funding support for the lead author was provided by the National Science Foundation Interdisciplinary Graduate Research and Training (IGERT) program under Grant 0221688 and by Texas Tech University.

REFERENCES

Anctil, F., and M. A. Donelan, 1996: Air–water momentum flux observations over shoaling waves. *J. Phys. Oceanogr.,* **26,** 1344–1353.

Arya, S. P., 1988: *Introduction to Micrometeorology*. Academic Press, 307 pp.

Barthelmie, R. J., J. P. Palutikof, and T. D. Davies, 1993: Estimation of sector roughness lengths and the effect on prediction of the vertical wind speed profile. *Bound.-Layer Meteor.,* **66,** 19–47.

Beljaars, A. C. M., 1987: The measurement of gusts at routine wind stations—A review. KNMI Scientific Rep. WR87-11, 50 pp.

Bendat, J. S., and A. G. Piersol, 1986: *Random Data: Analysis and Measurement Procedures.* John Wiley and Sons, 556 pp.

Black, P. G., and Coauthors, 2007: Air–sea exchange in hurricanes: Synthesis of observations from the coupled boundary layer air–sea transfer experiment. *Bull. Amer. Meteor. Soc.,* **88,** 357–384.

Counihan, J., 1975: Adiabatic atmospheric boundary layers: A review and analysis of data from the period 1880–1972. *Atmos. Environ.,* **9,** 871–905.

Dietrich, J. C., and Coauthors, 2011a: Hurricane Gustav (2008) waves and storm surge: Hindcast, synoptic analysis, and validation in southern Louisiana. *Mon. Wea. Rev.,* **139,** 2488–2522.

——, and Coauthors, 2011b: Modeling hurricane waves and storm surge using integrally-coupled, scalable computations. *Coastal Eng.,* **58,** 45–65.

Donelan, M. A., B. K. Haus, N. Ruel, W. J. Stianssnie, H. C. Graber, O. B. Brown, and E. S. Saltzman, 2004: On the limiting aerodynamic roughness of the ocean in very strong winds. *Geophys. Res. Lett.,* **31,** L18306, doi:10.1029/2004GL019460.

Garratt, J. R., 1977: Review of drag coefficients over oceans and continents. *Mon. Wea. Rev.,* **105,** 915–929.

Holmes, J. D., 2001: *Wind Loading of Structures*. Spon Press, 392 pp.

Hope, M. E., and Coauthors, 2013: Hindcast and validation of Hurricane Ike (2008) waves, forerunner, and storm surge. *J. Geophys. Res.,* doi:10.1002/jgrc.20314, in press.

Kaimal, J. C., and J. J. Finnigan, 1994: *Atmospheric Boundary Layer Flows: Their Structure and Measurement*. Oxford University Press, 289 pp.

Kennedy, A. B., and Coauthors, 2010: Rapidly installed temporary gauging for waves and surge, and application to Hurricane Gustav. *Cont. Shelf Res.,* **30,** 1743–1752.

Kudryavtsev, V. N., and V. K. Makin, 2007: Aerodynamic roughness of the sea surface at high winds. *Bound.-Layer Meteor.,* **125,** 289–303.

Letchford, C., A. Gardner, R. Howard, and J. Schroeder, 2001: A comparison of wind prediction models for transitional flow regimes using full-scale hurricane data. *J. Wind Eng. Ind. Aerodyn.,* **89,** 925–945.

Paulsen, B. M., and J. L. Schroeder, 2005: An examination of tropical and extratropical gust factors and the associated wind speed histograms. *J. Appl. Meteor.,* **44,** 270–280.

Peterson, E. W., 1969: Modification of mean flow and turbulent energy by a change in surface roughness under conditions of neutral stability. *Quart. J. Roy. Meteor. Soc.,* **95,** 561–575.

Powell, M. D., 2008: High wind drag coefficient and sea surface roughness in shallow water. NOAA/AOML Hurricane Research Division Final Rep. to the Joint Hurricane Testbed, 24 pp. [Available online at http://www.nhc.noaa.gov/jht/07-09reports/final_Powell_JHT08.pdf.]

——, and S. H. Houston, 1996: Hurricane Andrew's landfall in south Florida. Part II: Surface wind fields and potential real-time applications. *Wea. Forecasting,* **11,** 329–349.

——, S. Houston, and T. Reinhold, 1996: Hurricane Andrew's landfall in south Florida. Part I: Standardizing measurements for documentation of surface wind fields. *Wea. Forecasting,* **11,** 304–328.

——, L. Amat, and N. Morrisseau-Leroy, 1998: The HRD real-time hurricane wind analysis system. *J. Wind Eng. Ind. Aerodyn.,* **77–78,** 53–64.

——, P. J. Vickery, and T. A. Reinhold, 2003: Reduced drag coefficient for high wind speeds in tropical cyclones. *Nature,* **422,** 279–283.

——, and Coauthors, 2010: Reconstruction of Hurricane Katrina's wind fields for storm surge and wave hindcasting. *Ocean Eng.,* **37,** 26–36.

Savelyev, S. A., and P. A. Taylor, 2005: Internal boundary layers: I. Height formulae for neutral and diabatic flows. *Bound.-Layer Meteor.,* **115,** 1–25.

Schmid, H. P., and T. R. Oke, 1990: A model to estimate the source area contributing to surface layer turbulence at a point over patchy terrain. *Quart. J. Roy. Meteor. Soc.,* **116,** 965–988.

Schroeder, J. L., D. A. Smith, and R. E. Peterson, 1998: Variation of turbulence intensities and integral scales during the passage of a hurricane. *J. Wind Eng. Ind. Aerodyn.,* **77–78,** 65–72.

Simiu, E., and R. H. Scanlan, 1986: *Wind Effects on Structures: An Introduction to Wind Engineering*. 2nd ed. John Wiley and Sons, 589 pp.

Stull, R. B., 1988: *An Introduction to Boundary Layer Meteorology.* Kluwer Academic, 680 pp.

Weiss, C. C., and J. L. Schroeder, 2008: StickNet: A new portable rapidly deployable surface observations system. *Bull. Amer. Meteor. Soc.,* **89,** 1502–1503.

Wood, D. H., 1982: Internal boundary layer growth following a step change in surface roughness. *Bound.-Layer Meteor.,* **22,** 241–244.

Copyright of Journal of Applied Meteorology & Climatology is the property of American Meteorological Society and its content may not be copied or emailed to multiple sites or posted to a listserv without the copyright holder's express written permission. However, users may print, download, or email articles for individual use.